




Article

# Preparation and Characterization of Chitosan Coated PLGA Nanoparticles of Resveratrol: Improved Stability, Antioxidant and Apoptotic Activities in H1299 Lung Cancer Cells

Hibah M. Aldawsari <sup>1,\*</sup> , Nabil A. Alhakamy <sup>1</sup> , Rayees Padder <sup>2</sup> , Mohammad Husain <sup>2</sup> and Shadab Md <sup>1,\*</sup> 

<sup>1</sup> Department of Pharmaceutics, Faculty of Pharmacy, King Abdulaziz University, Jeddah 21589, Saudi Arabia; nalhakamy@kau.edu.sa

<sup>2</sup> Department of Biotechnology, Jamia Millia Islamia (Central University), New Delhi 110025, India; prayees26@gmail.com (R.P.); mhusain2@jmi.ac.in (M.H.)

\* Correspondence: haldosari@kau.edu.sa (H.M.A.); shaque@kau.edu.sa (S.M.)

Received: 13 April 2020; Accepted: 27 April 2020; Published: 29 April 2020



**Abstract:** Resveratrol (RES) is a polyphenolic compound which has shown beneficial pharmacological effects such as anti-inflammatory, antioxidant, and anti-cancer effects. However, poor aqueous solubility, bioavailability, and low stability are the major limitations to the clinical application of RES. Therefore, in the present study, chitosan (CS) coated PLGA nanoparticles of RES (CS-RES-PLGA NPs) was developed, characterized and its anticancer activity was evaluated in the H1299 lung carcinoma cell line. The effects of the increase in CS coating and cryoprotectant concentration on particle size, polydispersity index (PDI) and zeta potential (ZP) were determined. The particle size, PDI, ZP and entrapment efficiency of the optimized CS-RES-PLGA NPs were found to be  $341.56 \pm 7.90$  nm,  $0.117 \pm 0.01$ ,  $26.88 \pm 2.69$  mV and  $75.13\% \pm 1.02\%$  respectively. The average particle size and ZP showed a steady increase with an increase in CS concentration. The increase in positive zeta potential is evident for higher CS concentrations. The effect of trehalose as cryoprotectant on average particle size was decreased significantly ( $p < 0.05$ ) when it was increased from 1%–5% *w/v*. TEM and SEM showed uniform particle distribution with a smooth surface and spherical shape. The CS coating provides modulation of in vitro drug release and showed a sustained release pattern. The stability of RES loaded PLGA NPs was improved by CS coating. CS-coated NPs showed greater cytotoxicity and apoptotic activities compared to free RES. The CS coated NPs had a higher antioxidant effect than the free RES. Therefore, CS coated PLGA NPs could be a potential nanocarrier of RES to improve drug solubility, entrapment, sustain release, stability and therapeutic application.

**Keywords:** resveratrol; PLGA nanoparticles; chitosan; coating; apoptosis; cell viability

## 1. Introduction

Resveratrol (RES) is a polyphenolic compound, abundantly available in various foods, such as berries, peanut and grapes. RES is chemically 3,4',5-trihydroxy-trans-stilbene, produced by the plant because of bacterial and fungi attack [1]. RES recently attracted tremendous research attention for its pharmacological potential, where it has reported to possess antiaging, anti-inflammatory, antioxidant, anticancer, antidiabetic, neuroprotective and cardioprotective effects [2–5]. Unfortunately, the major drawbacks of RES limit its' clinical applicability due to poor aqueous solubility, low chemical stability, short plasma half-life, extensive metabolism in liver and poor bioavailability. The systemic availability

of RES is quite low after the oral administration of high doses [4,6]. Therefore, the solubility and bioavailability of RES require more consideration in the development of suitable formulations.

Nanocarrier-based drug delivery systems have been developed to deliver encapsulated drug(s) to the desired site without compromising stability; these formulations release drug(s) in a specific area or organ in a more stable and controlled way for the effective and safe treatment of cancer [7]. Much attention has been centered on the development of biodegradable polymeric NPs due to their higher bioavailability and greater safety. Various nanocarriers for the delivery of RES were developed such as albumin-based nanoparticles (NPs) of RES were found to inhibit the growth of human primary ovarian carcinoma cells implanted in nude mice [8]. Additionally, encapsulation of RES in gelatin NPs reported exhibiting greater stability, enhanced cellular uptake, improved efficacy against lung cancer cells compared to free RES, without producing any toxicity [9]. Furthermore, solid lipid NPs of RES have shown superior ability towards inhibition of MDA-MB-231 cell proliferation, indicating the potential of developed nanoformulation in breast cancer therapy [10]. Among the various polymeric NPs PLGA was used to develop NPs due to its biodegradability, biocompatibility and is generally recognized as safe [11]. PLGA has been used as an effective carrier to deliver anticancer drugs [11]. In this context, PLGA NPs of RES were also developed to improve programmed cell death in a prostate cancer cell line (LNCaP) [11]. Similarly, chitosan (CS) is one of the most acceptable natural polymers for use as a nanocarrier to deliver chemotherapeutic drugs to the target site [12]. Miele and co-workers have developed chitosan oleate (CS-OA) assembled polymeric micelles and PLGA using chitosan oleate (CS-OA) as a coating material to load poorly soluble drug [13]. They showed that RES stability was more profound in loading in PLGA NPs as compared to polymeric micelles [13]. Sanna and co-workers have developed blend of cationic (chitosan) and anionic (alginate) coated PLGA NPs for improvement in drug release in a controlled manner and photostability [14]. Wang and co-workers have developed chitosan-coated PLGA nanoparticles of where they demonstrated neuro-protective action of the prepared nanoparticles and functional recovery of the spinal cord after injury. They showed that the prepared nanoparticles have significantly improved anti-inflammatory cytokine (IL-10) and reduced the level of inflammatory cytokines [15]. However, there is no previous report has published on chitosan-coated PLGA NPs of resveratrol for improvement apoptotic activity in lung cancer cells.

Therefore, the objective of the present study was to developed RES-PLGA NPs and CS-coated RES-PLGA NPs for effective and sustained delivery of RES. To achieve our objective, prepared NPs were characterized for their size, surface charge, surface morphology, entrapment efficiency and in vitro release in different media. The effect of the increase in CS coating and cryoprotectant concentration on particle size, polydispersity index (PDI) and ZP were evaluated. The stability study of RES encapsulated in CS coated PLGA NPs was evaluated as compared to free RES. The antioxidant activity of prepared CS-RES-PLGA NPs was determined as compared to free RES. The in vitro evaluation of CS coated PLGA was performed using the H1299 lung cancer cell line to evaluate cytotoxicity, apoptotic activity, signaling pathway and cell cycle analysis.

## 2. Materials and Methods

### 2.1. Materials

RES, PLGA with lactide:glycolide of 50:50, the molecular weight of 40,000–75,000 Da, CS (75%–85% deacetylated, average MW 50,000 Da) were purchased from Sigma-Aldrich, St. Louis, MO, USA. The apoptosis detection kit was purchased from BD Bioscience. Bax, B-actin, and Bcl2 primary antibodies were purchased from Novus Biologicals (Centennial, CO, USA). All other chemicals used were of analytical grade.

### 2.2. Cell Lines

Human non-small cell lung carcinoma (NSCLC) cell line (H1299) was obtained from National Centre for Cell Science (NCCS), Pune, India. These cells were cultured in Dulbecco's Modification of

Eagle's Medium (DMEM) supplemented with  $100 \text{ mg}\cdot\text{mL}^{-1}$  streptomycin, 10% fetal bovine serum (FBS) and  $100 \text{ U}\cdot\text{mL}^{-1}$  penicillin, at  $37^\circ\text{C}$  in a 5%  $\text{CO}_2$  incubator with 95% humidity. Cells were subcultured to achieved 80%–90% confluence for experiments.

### 2.3. Preparation of RES-PLGA NPs and CS Coated RES-PLGA NPs

RES-PLGA NPs were formulated adopting the single emulsion-sonication method with slight modification [16]. The organic phase was prepared by dissolving the polymer (PLGA) in dichloromethane ( $50 \text{ mg/mL}$ ). RES was dissolved in the organic phase ( $10 \text{ mg/mL}$ ). Afterwards, 2 mL of the organic phase was added dropwise into an aqueous phase consisted of 10 mL of 1% PVA solution under magnetic stirring at 600 rpm for 1 h. Afterward, it was homogenized using a probe sonicator for 5 min at 40% power. The organic phase was allowed to evaporate overnight under magnetic stirring at room temperature. Evaporation of the volatile organic phase results in precipitation of NPs, which were recovered by ultracentrifugation (Beckman Coulter, Optima LE 80K, Brea, CA, USA) at  $11,200\times g$  for 30 min at  $4^\circ\text{C}$ . The precipitated NPs were then washed with deionized water and centrifuged again to obtain NPs and the collected supernatant was used to determine entrapment efficiency. The NPs pellet was redispersed in deionized water and the cryoprotectant (Trehalose 5%,  $w/v$ ) was added before freeze-drying for 24 h to obtain freeze-dried NPs for further use.

CS-coated RES-PLGA NPs were prepared using the above-mentioned method with minor modification. In the CS coated nanoformulation, the aqueous phase consisted of 10 mL of CS solution and 1% PVA solution prepared in acetic acid solution (1%  $v/v$ ). The concentration of CS in the aqueous phase was varied from 0.1% to 1%  $w/v$  to obtain NPs with different particle size, polydispersity index, and zeta potential. Blank NPs were prepared with the same method without using drug RES.

### 2.4. Characterization of the Nanoparticles

#### 2.4.1. Mean Particle Size, Size Distribution, and Zeta Potential

Hydrodynamic particle size and size distribution of the NPs was determined by the dynamic light scattering (DLS) technique (Zetasizer Nano-ZSP (Malvern Instruments, Worcestershire, UK) [17]. All measurements were performed at room temperature ( $25 \pm 2^\circ\text{C}$ ), a laser wavelength of 673 nm with a scattering angle of  $173^\circ$  [17]. The PDI indicates the size distribution of NPs. NP suspensions were diluted in distilled water (1:20  $v/v$ ) and placed in a cuvette for analysis. Zeta potential of suspended NPs was determined by electrophoretic light scattering (ELS) method. NP samples were diluted appropriately in phosphate buffer saline and placed in an electrophoretic cell at  $25^\circ\text{C}$ . CS coated PLGA NPs and PLGA NPs were measured for size, PDI and zeta potential. Measurements were performed in triplicate and expressed as mean  $\pm$  SD.

#### 2.4.2. Electron Microscopy Evaluation

The shape and monodispersity of CS coated PLGA NPs were determined by transmission electron microscopy (TEM) (JEOL JEM1010, Tokyo, Japan) and scanning electron microscopy (SEM) (Zeiss EVO LS10, Cambridge, UK). For TEM analysis, a drop of NP dispersion in water was placed and mounted on a formvar coated copper grid. The thin layer of the sample was stained with phosphotungstic acid (1%  $w/v$ ), the excess sample was removed with filter paper and samples were air-dried for 2 h. The dried samples were then visualized under TEM to observe the actual size and shape of the formulations. In SEM analysis, the monolayer of the NPs was fixed on a metallic slab where the particles were coated with a thin film of gold (10 nm) using the gold sputter technique [17]. Thereafter the CS-coated NPs were analyzed under the SEM (Zeiss EVO LS10 Cambridge, UK) at 15 keV.

### 2.5. Entrapment Efficiencies of CS-RES-PLGA NPs

The entrapment efficiency (%EE) of the drug (RES) within the polymeric NPs was determined in accordance with previously published methods [18] through the measurement of RES concentration

in the dispersed medium during the formulation process. In due course, the supernatant solution of the harvested NPs was collected following ultracentrifugation (Beckman Coulter, Optima LE 80K, Brea, CA, USA) at  $11,200\times g$  for 30 min at 25 °C. The concentration of drug in the supernatant was determined at 304 nm using a double beam UV–visible spectrophotometer. The calculation of %EE was made using the following formula:

$$\%EE = \frac{W_t(\text{mg}) - W_f(\text{mg})}{W_t} \times 100\%$$

where  $W_f$  is the free drug present in the supernatant and  $W_t$  is the total drug in the organic solution for drug loading.

## 2.6. In Vitro pH Controlled Release Study of RES from the PLGA NPs and CS-PLGA NPs

The in vitro release of RES from the RES-PLGA NPs and CS-PLGA NPs was performed in two different release media with pH 7.4 and pH 5.5 in order to simulate physiologic and acidic conditions of cancer cells with slight modification [19]. Equal quantities of RES-PLGA NP samples were packed in a dialysis sac and suspended in 25 mL of the respective release media (pH 5 or pH 7.4). A similar set of release studies of the CS-coated RES-PLGA NP samples was undertaken. The temperature was maintained at 37 °C in a paddle-type dissolution apparatus, where the speed of the paddle was set to 100 rpm. At a particular time intervals, 1 mL sample aliquots were collected and replaced with an equal volume of fresh buffer. The quantity of drug present in the release medium was evaluated using HPLC.

## 2.7. Stability Study

The CS-RES-PLGA-NPs were freeze-dried and dispersed in phosphate buffer saline pH 7.4, protected from light and stored at 4 °C for three months. NPs were assayed at the time points of zero, one and three months, for determination of particle size, PDI and zeta potential [20]. The chemical stability against isomerization of free RES and CS-RES-PLGA-NPs were exposed to UV light at 365 nm. The free RES and freeze-dried NPs dispersed in PBS samples were taken at 0.5, 1, and 2 h and further diluted for the quantitation of RES.

## 2.8. Antioxidant Activity

The antioxidative activity of the formulations was determined using 2,2-diphenyl-1-picrylhydrazyl (DPPH) scavenging assay method described previously with a small modification [21]. CS-RES-PLGA NPs, free RES and gallic acid (positive control) were prepared in ethanol solution at different concentrations ranging from 5–50 µg/mL. Gallic acid was used as a positive control. We prepared 2 mL of a 0.1 mM DPPH-ethanol solution and mixed with 2 mL of different concentrations of prepared formulations. The mixed solutions are vortexed thoroughly, incubated at room temperature in the dark for 30 min, and followed by measuring the absorbance using a UV–Vis spectrophotometer (UV-2600, Shimadzu, Tokyo, Japan) at a wavelength of 520 nm in triplicate. The DPPH scavenging percentage was calculated using the following equation:

$$\text{DPPH scavenging percentage (\%)} = \frac{\text{Absorbance control} - \text{Absorbance test}}{\text{Absorbance control}} \times 100\%$$

## 2.9. Cell Viability Assay of Prepared RES Nanoparticles

Prediction of cytotoxicity of investigational agents in different cells is among the first in vitro bioassay techniques, which usually provides the basis of crucial means of screening and safety assessment of the investigational agent. Therefore, the MTT colorimetric assay was conducted in NSCLC cell line (H1299) with free RES, RES-PLGA NPs, CS-RES-PLGA NPs and blank CS-PLGA NPs (without drug). We seeded  $3 \times 10^4$  H1299 cells in each well of the 96-well plate for a period of 24 h. The incubated cells were then treated with different concentrations (5–100 µg/mL) of free RES,

RES-NP, and blank CS-PLGA NPs. Following an incubation period of 24 h, the treated samples were removed from the wells and the cells were incubated with 25  $\mu$ L of MTT solution (0.5%, *w/v*) for 4 h at 37 °C. After incubation, the unreacted MTT solution was removed and the cells were exposed to 150  $\mu$ L DMSO in each well for a period of 20 min to solubilise the formed formazan crystals. Finally, the absorbance of the formazan solution in each well was measured at 570 nm using a microplate reader (Thermo Fisher Scientific, Waltham, MA, USA); the absorbance was proportional to the number of viable cells in the wells [22].

#### 2.10. Apoptosis in H1299 Cells by Free RES and CS-RES-PLGA NPs (RES-NPs)

A double-staining technique was used to analyze the apoptotic potential of free RES and RES-NPs. The  $6 \times 10^3$  cells H1299 cells were seeded in 6-well plates where they were incubated with free RES and RES-NPs [22,23]. Following incubation of 24 h, the cells were washed twice with cold phosphate buffer saline. The cells were then re-suspended in binding buffer and stained with 5  $\mu$ L of Annexin V-FITC and 5  $\mu$ L of propidium, incubated for 15 min at room temperature and then analyzed by flow cytometry (BD FACS AriaTm III).

#### 2.11. Western Blotting

The effect of RES and RES NPs on the expression of apoptotic protein markers (Bax and Bcl-2) in H1299 lung cancer cells was assessed by western blot [22,23]. The  $6 \times 10^3$  H1299 cells were seeded in 6-well plates and incubated with formulations for 24 h. The cells were washed twice with PBS and incubated on ice in RIPA lysis buffer for 30 min. Liquid-containing proteins were obtained by collecting the supernatant after centrifugation (12,000 rpm at 4 °C). The extracted proteins were separated using SDS-PAGE and transferred to PVDF membranes. The blocking agent (TBST with 5% BSA) was applied for 2 h to block unspecific binding sites. The membrane was then incubated with primary antibodies to BAX, Bcl-2 and  $\beta$ -actin. After 10 h, the membrane was incubated with secondary antibodies for 1 h and then washed with TBST and blots were detected using a chemiluminescence reagent kit and quantification was performed by densitometric analysis using image J software (1.52t, NIH, MD, USA).

#### 2.12. RES and RES-NPs Induced Cell Cycle Analysis

H1299 cells were used to determine the effect of free RES and RES NPs on cell cycle distribution [23]. The  $6 \times 10^3$  cells were incubated in 96-well plate with a fixed concentration of RES in different formulations. The cells were then harvested and fixed with 70% ethanol at 4 °C for 30 min. The cells were washed twice with phosphate buffer saline and stained with 50 mg/mL propidium iodide solution containing 50 ng/mL of RNase for 30 min in dark at room temperature and then cell cycle was analyzed using a flow cytometer (BD FACS AriaTm III, Franklin Lakes, NJ, USA).

#### 2.13. Statistical Analysis

Statistical analysis was performed by Student's t-test between two groups and one-way ANOVA for multiple groups followed by Tukey's post hoc test. All results are given as mean  $\pm$  SD. Differences are considered statistically significant at a level of  $p < 0.05$ .

### 3. Results and Discussion

#### 3.1. Development of RES-PLGA NPs and CS Coated RES-PLGA-NP

PLGA NPs were prepared using PLGA and PVA through the single emulsion-sonication method, where PVA acts as a stabilizer of the formulation. Ultrasonication helped to reduce the size of the particles to the nanometer-sized range with a narrow PDI. Sizes of the PLGA-NPs were measured as  $271.63 \pm 13.81$  nm, where the entrapment of the drug did not show any significant ( $p > 0.05$ ) increase in the size of the NPs. However, a significant ( $p < 0.05$ ) increase in the size of the particles was found ( $341.56 \pm 7.90$  nm) when the NPs were placed in a CS solution (Table 1). Incorporation of RES within



the nanostructure was shown to increase the PDI of the formulation significantly ( $p < 0.05$ ); however, all the formulated particles showed a PDI  $< 0.4$ , indicating the monodisperse nature of the particles. As depicted in Figure 1 and Table 1, the surface charge of the formulated PLGA NPs was found to be almost constant, slightly negative or near neutral (e.g.,  $-4.16 \pm 1.13$  mV for RES-PLGA NPs). Coating of the NPs with CS, in comparison, produced a significant alteration of the surface charge towards the positive to  $+26.88 \pm 2.69$  mV (for CS coated RES-PLGA NPs-CS) (Figure 1). With the change in concentration of PLGA, the %EE of RES was varied proportionately (data not shown) within the PLGA-NPs; however, the optimized formulation of CS-coated RES-PLGA-NPs was found to encapsulate  $75.13\% \pm 1.02\%$ .

**Table 1.** Characterization parameters of optimized formulations.

Formulations	Average PS (nm) $\pm$ SD	Average PDI $\pm$ SD	Average ZP (mV) $\pm$ SD	Average EE (%) $\pm$ SD
PLGA NPs	271.63 $\pm$ 13.81	0.123 $\pm$ 0.08	$-2.55 \pm 0.28$	NA
RES-PLGA NPs	286.13 $\pm$ 11.64	0.351 $\pm$ 0.02	$-4.16 \pm 1.13$	71.25 $\pm$ 0.67
CS-PLGA NPs	349.10 $\pm$ 17.92	0.358 $\pm$ 0.01	$29.3 \pm 0.60$	NA
CS-RES-PLGA NPs	341.56 $\pm$ 7.90	0.117 $\pm$ 0.01	$26.88 \pm 2.69$	75.13 $\pm$ 1.02

Results expressed as mean  $\pm$ SD ( $n = 3$ ). SD: standard deviation; NA: not applicable; NPs: nanoparticles. RES: resveratrol, CS: chitosan.

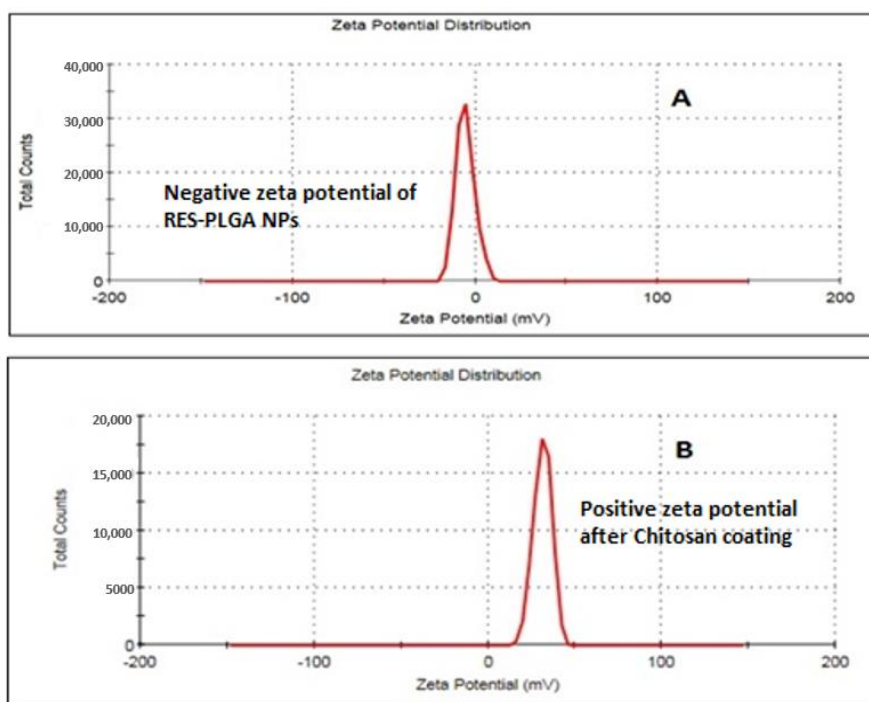


**Figure 1.** Zeta potential of PLGA nanoparticles (NPs) suspended in PBS (pH = 7.4), (A) Resveratrol (RES)-PLGA-NPs; (B) Chitosan (CS)-coated RES-PLGA-NPs.

### 3.2. Effect of Increase in CS Concentration on Particle Size, PDI, and Zeta Potential

The effect of the CS concentration of various parameters of CS coated PLGA NPs was studied. The results of the studies are shown in Figure 2. The average particle size showed a steady increase in increasing CS concentration. The average particle size was  $287.5 \pm 5.46$  nm when CS concentration was 0.1% *w/v*. This value reached  $458.7 \pm 10.57$  when the CS concentration was 1.0%. Meanwhile, the PDI values did not show any such trend dependent on CS concentration. The PDI values were sufficiently low ( $< 0.2$ ) till 0.75% of CS. The PDI at 1.0% CS was still at an acceptable value of  $0.26 \pm 0.04$ . In the case of zeta potential values, the results were as expected. The values of zeta potential increased proportionally to the concentration of CS used for coating. The zeta potential was  $11.3 \pm 4.30$  at 0.1%

CS concentration, which changed to  $18.2 \pm 1.51$ ,  $26.9 \pm 2.69$ ,  $29.3 \pm 4.55$ , and  $34.9 \pm 1.73$  mV for CS concentrations of 0.25%, 0.50%, 0.75%, and 1.00% w/v, respectively.

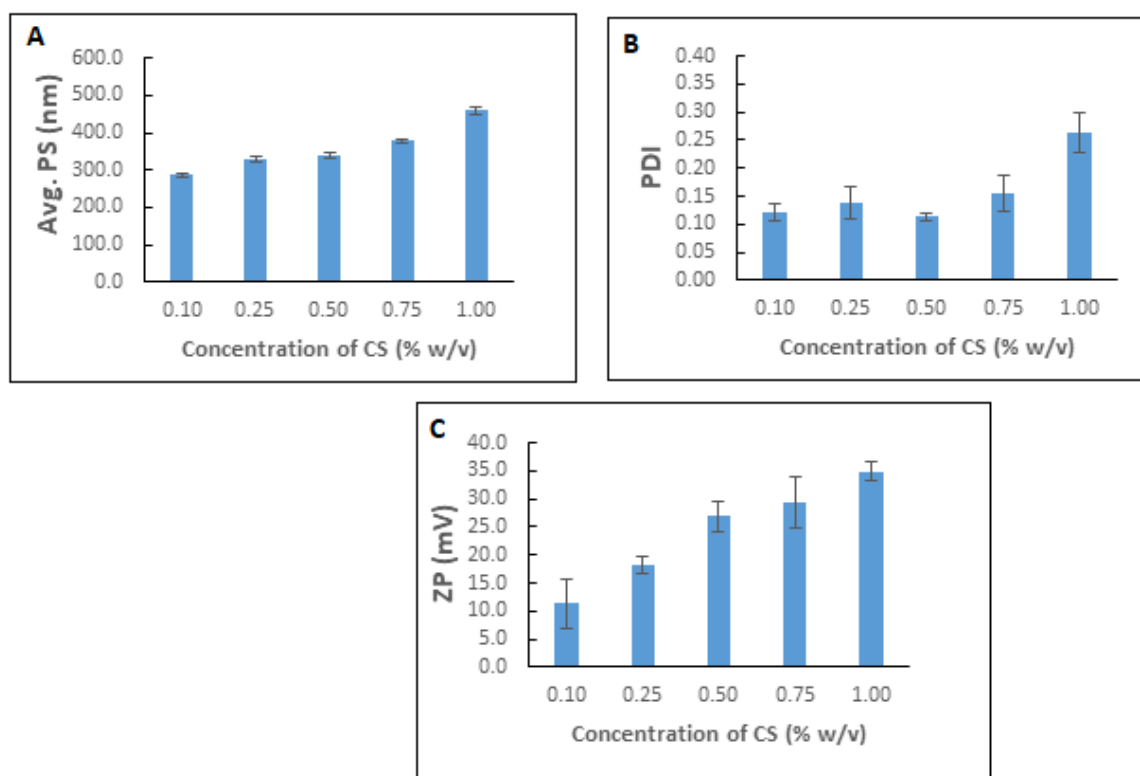


**Figure 2.** Effect of CS concentration on various parameters (A) particle size; (B) PDI; (C) ZP of CS-RES-PLGA NPs.

CS-coated PLGA NPs are widely studied for the delivery of a variety of therapeutic agents and different purposes [24,25]. While PLGA NPs are excellent in biocompatibility and biodegradability, a coating of CS usually provides bioadhesive properties to the NPs. Such a system has added advantages in drug delivery. A simple PLGA nanoparticulate system suffers several disadvantages. Burst drug release, poor interaction with cells or proteins, and poor drug targeting are some among them [24]. Besides, the positively charged CS coating offers several advantages such as enhanced cellular uptake [25].

The study of the effect of surface modification by CS has been an area of interest in many reported studies. In our study, we tried to find out the influence of various CS concentrations on the average particle size, PDI, and zeta potential of the CS-coated RES-loaded PLGA NPs. A gradual increase in the average particle size was observed in our results. It was as expected from the process of CS coating. A higher concentration of CS solution would result in the thicker coating over the PLGA NPs and thus an increase in the particle size. Similar results are reported by many studies [24,26]. The very low PDI values implied a narrow particle size distribution obtained by the procedure employed. CS coating over PLGA NPs has previously reported producing PDI values well below 0.2 even when high concentrations of CS are used [24,25]. Therefore, such an independency of PDI on CS concentration could be expected.

The cationic nature and subsequently the positive charge of CS polymer are well known, while PLGA produces NPs with a negative zeta potential [24]. The cationic nature of CS favors the coating over negatively charged PLGA NPs. Therefore, it could be expected that at higher concentrations of CS, the number of molecules coated on the PLGA NPs would be higher. Thus, the surface charge

would be more positive at higher concentrations of CS. This is evident from the increased positive zeta potential values for higher CS concentrations. This type of effect of CS coating is well established [24].

### 3.3. Effect of Cryoprotectant Concentration

The effect of trehalose as cryoprotectant on average particle size, PDI and zeta potential are shown in Figure 3. The particle size was found to decrease on increasing the concentration of trehalose. The decrease was significant up to 5%. The particle size was  $493.2 \pm 16.73$  nm for 1% trehalose. Later it reached  $341.6 \pm 7.54$  nm when the concentration reached 5%. When the trehalose concentration was changed to 10%, the particle size was found to be  $355.0 \pm 10.87$  nm. Thus, only a slight increase ( $p > 0.05$ ) was observed when the trehalose concentration was changed from 5% to 10%. A similar pattern was observed for PDI too. The PDI also decreased from 1% trehalose ( $0.32 \pm 0.02$ ) to 5% trehalose ( $0.11 \pm 0.01$ ). Thereafter an increase in PDI to  $0.15 \pm 0.02$  was shown by 10% trehalose. The zeta potential was found to increase on higher concentrations of trehalose in contrast to an expected decrease in positive surface charge. The zeta potential was  $7.1 \pm 1.1$  mV for 1% trehalose, which eventually increased to  $27.4 \pm 1.9$  mV for 10% trehalose.

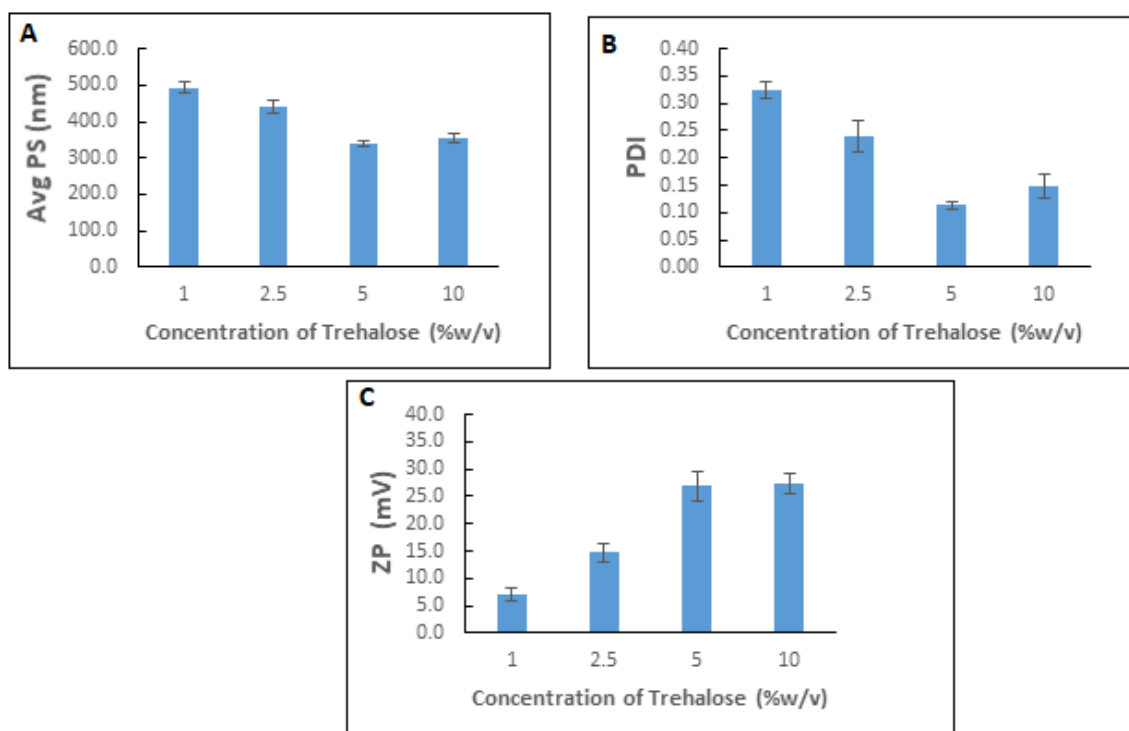


**Figure 3.** Effect of trehalose as cryoprotectant on (A) particle size, (B) polydispersity index (PDI), and (C) zeta potential. There was no significant difference ( $p > 0.05$ ) was observed for zeta potential at 5% and 10% of trehalose).

The process of freeze-drying improves the stability of NPs and is important in the conservation of their physical and chemical characteristics and providing long-term stability. Difficulties in re-dispersion is another challenge when freeze-drying of NPs is carried out in the absence of any cryoprotectant [27]. Further, the size and size distribution of the freeze-dried NPs also depend on the use of a cryoprotectant. Cryoprotection renders stability during the freeze-drying process. The absence of a cryoprotectant during the freeze-drying process produces larger particles with a high tendency for aggregation [27].

Sugars are widely used as cryoprotectants for NPs [28]. Therefore, in the present study, the effect of trehalose as cryoprotectant was studied through concentrations of 1%–10% w/v. It was observed that the average particle size was decreased significantly ( $p < 0.05$ ) when trehalose was increased from 1%–5% w/v. Obviously, towards the final stages of the process of freeze-drying, a high concentration of



NPs and excipients occur. This could trigger the aggregation of the NPs. This could result in irreversible fusion and destabilization of NPs [29]. Thus, the presence of trehalose has offered protection and stability to the NPs at this cryo-concentrated phase to finally result in lower particle size. This effect of sugars like trehalose results from the formation of an amorphous glassy layer around the NPs [30]. When we consider the higher average particle size on the use of trehalose at 10% *w/v* compared to lower concentrations, it is reported that higher concentrations of cryoprotectant could lead to aggregation [27]. Similar effects in trehalose were seen in previous studies as well [31]. The enhancement of resistance to particle movement by the formation of thicker amorphous trehalose coating around the NPs could have resulted in such a result in our study. This thicker coating reduces the movement (dynamics) of the particles and thus results in a higher particle size output.

The effect of cryoprotectants on PDI is similar to their effect on particle size. A distinct concentration-dependent effect of trehalose was observed on PDI. Such results are observed in previous studies too [27]. As mentioned previously, the effect of trehalose as a cryoprotectant has reduced the PDI values at higher concentrations of trehalose. A reduction in the aggregation of NPs would automatically result in lower PDI values. Thus, it is obvious that the PDI would follow a pattern similar to the average particle size.

The zeta potential was found to increase up to 5% concentration and remained almost the same at 10%. There was no significant difference ( $p$ -value > 0.05) between the zeta potentials at 5% and 10% *w/v* concentrations. Trehalose is reported to increase negative-charged zeta potential when used as lyoprotectant or cryoprotectant [32]. Thus, we expected such a result in our studies as well, with trehalose as a cryoprotectant. However, rather than a decrease in zeta potential (increase in negative-zeta potential), we observed an increase in zeta potential (increase in positive-zeta potential). The cryoprotection might have retained higher quantities of CS on the surface of the PLGA nanoparticles resulting in higher zeta potential. Another possibility is that trehalose molecules get entrapped inside the CS molecules. This might have masked the effect of trehalose on zeta potential. A change in CS conformation leaving more available amine groups at the NP's surface would be another possibility. All these could result in a positive surface charge. At this point in the discussion, it would be imperative to mention that the mechanism of cryoprotection of trehalose is still under controversy and unconfirmed [33]. Nevertheless, irrespective of charge, a higher zeta potential value indicates higher stability. Thus, it is consistent with the observations of particle size and PDI.

#### 3.4. Characterization of CS Coated RES-PLGA NPs

SEM and TEM images of the CS coated RES-PLGA NPs (Figure 4) shows that the NPs were spherical in morphology. The TEM image (Figure 4A) shows uniform particle size distribution. The SEM image (Figure 4B) confirmed the spherical morphology of the CS-RES-PLGA NPs.

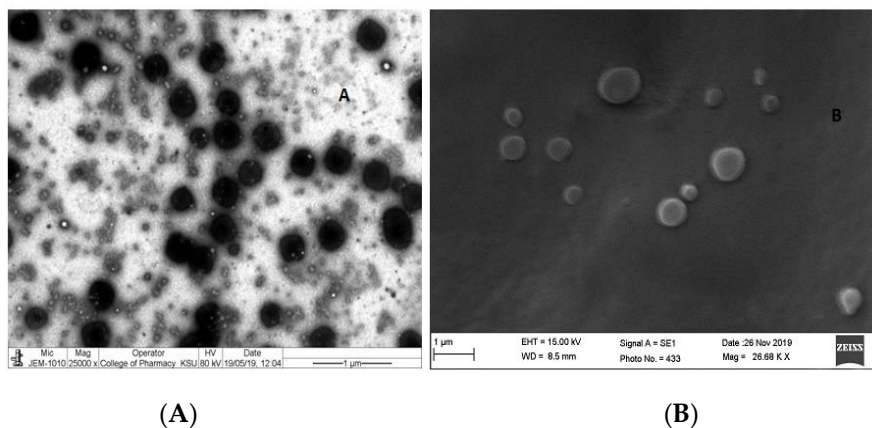


**Figure 4.** Particle size distribution, shape, and morphology of CS coated RES-PLGA-NPs. (A) Transmission electron microscopy (TEM) image (B) SEM image.

The SEM and TEM images of the CS-RES-PLGA NPs were consistent with the expectations. The particle size observed in the images was matching the observed average particle size measured with particle size analyzer. In the TEM image, a halo-like appearance was noted corresponding to the CS coating of the RES-PLGA NPs. The coating of CS occurs due to the electrostatic interactions of negatively charged PLGA NPs with the cationic CS polymer [24]. The carboxylic acid groups of PLGA and amine groups of CS favors such favorable electrostatic interactions. The SEM image shows a smooth surface of the particles. Both the SEM and TEM images were similar to reported CS-coated PLGA NPs [34].

### 3.5. Stability Study of CS-Coated RES-PLGA NPs

The storage stability study results after storage in phosphate buffer saline pH 7.4 at 4 °C are shown in Figure 5. The particle size was seen to have a slight and steady increase in storage. However, the increase in particle size was not significant ( $p > 0.05$ ) for adjacent sampling points. The initial particle size was  $341.56 \pm 7.90$  nm, which reached a value of  $367.27 \pm 2.71$  nm on storage for 90 days. The PDI values after different storage intervals did not show any regular pattern. Instead, all the values were below 0.22. At the same time, zeta potential values were showing marked change after storage. A decrease in the positive zeta potential values was noted when compared to the original value of  $26.88 \pm 2.69$  mV. The zeta potential values after storage for 30, 60, and 90 days show a gradual decrease, but the values were close to each other. After 90 days, the value reached the lowest with  $20.3 \pm 1.11$  mV.

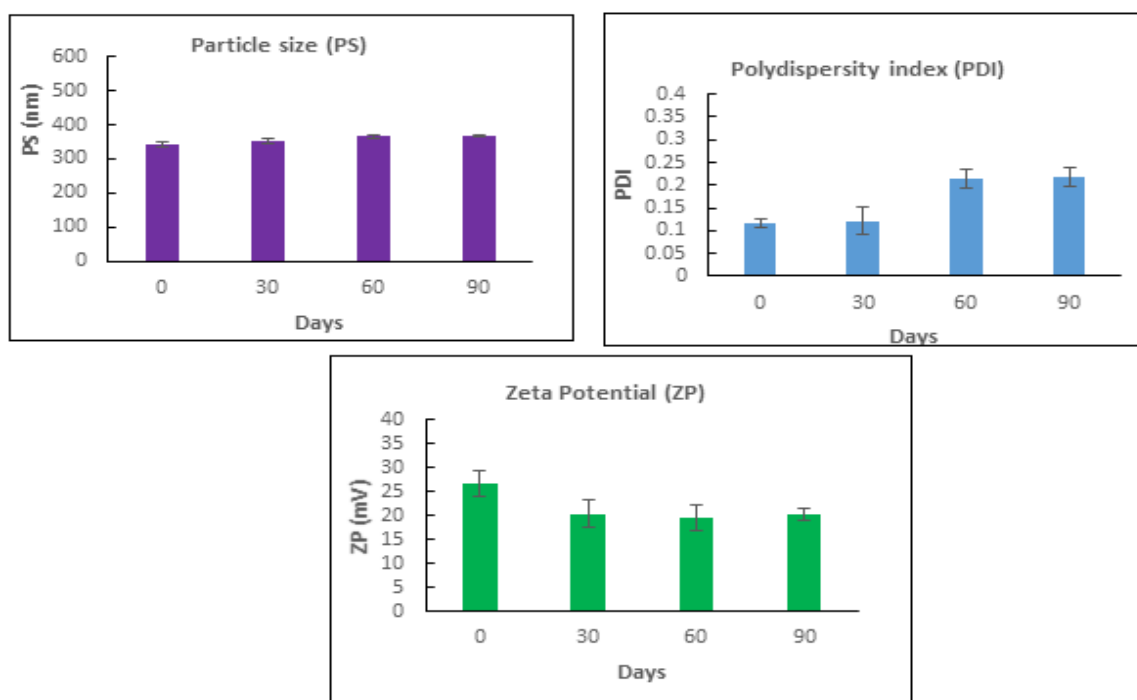


**Figure 5.** Bar diagrams of the results of storage stability studies of CS coated RES-PLGA NPs at 4 °C for 90 days in phosphate-buffered saline pH 7.4.

The storage stability studies with CS-RES-PLGA NPs show promising results. The storage stability studies are important to confirm that the formulation characteristics which influence their performance remain in an acceptable range after storage. The storage stability study was done in phosphate buffer saline pH 7.4 at 4 °C. In our study, the average particle size, PDI, and zeta potential results demonstrated that CS-RES-PLGA NPs possess storage stability. The particle size showed a gradual increase in storage. However, the increase in particle size was not very high. The maximum particle size obtained was  $367.27 \pm 2.71$  nm and was still in an acceptable range. Stability studies of similar CS-coated PLGA

NPs are reported to show a slight increase in particle size on storage [34]. The slight swelling of CS polymer, when suspended in the buffer, is assumed to result in such an increase in the particle size. The PDI values were very low even after storage for three months. This further indicated the absence of any serious aggregation of particles that would convert the sample to a collection of particles with different particle size ranges contributing to high polydispersity. In previous reports too CS-coated PLGA NPs have maintained low PDI even after storage for one year [35]. In the case of zeta potential, the value shows a slight decrease even upon storage for one month. Later the value remained similar till 3 months. It is known that the surface amine groups contribute to the positive charge of CS NPs. During storage, the particles come close to each other and subsequently result in larger particle sizes. In our study, a slight and steady increase in particle size was noted upon storage. This might have contributed to a slight lower zeta potential for CS-RES-PLGA NPs after storage. A similar observation was noted in the results of reported CS NPs, where the authors observed a drastic decrease in zeta potential within one month of storage [36].

The results of comparative photostability studies of encapsulated and free RES are shown in Figure 6. A gradual decrease in percent trans-RES was seen on exposure to UV light at 365 nm. After 0.5 h, the value for RES was  $73.13 \pm 2.50$  while for RES NPs it was  $82.82\% \pm 2.48\%$ . The percent of trans-RES remaining reached values of  $43.33 \pm 2.73$  and  $69.85\% \pm 2.18\%$  in RES and RES NPs samples after 2 h.

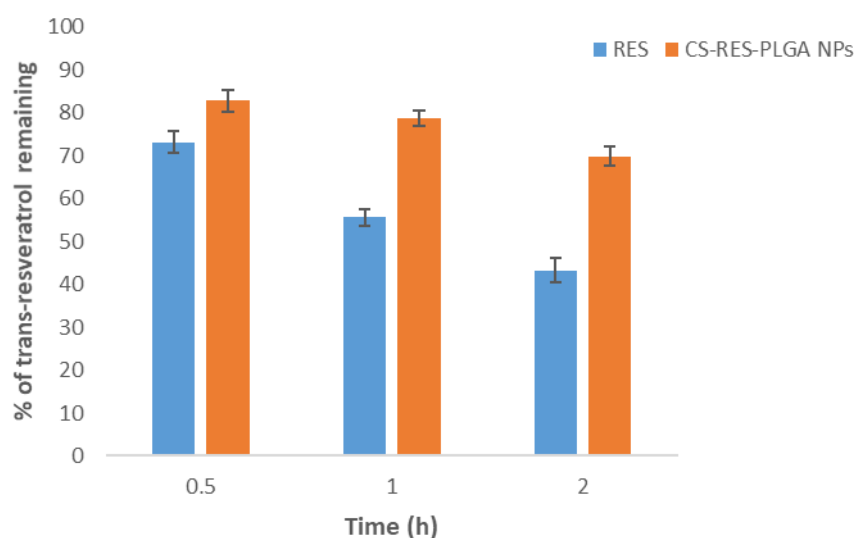
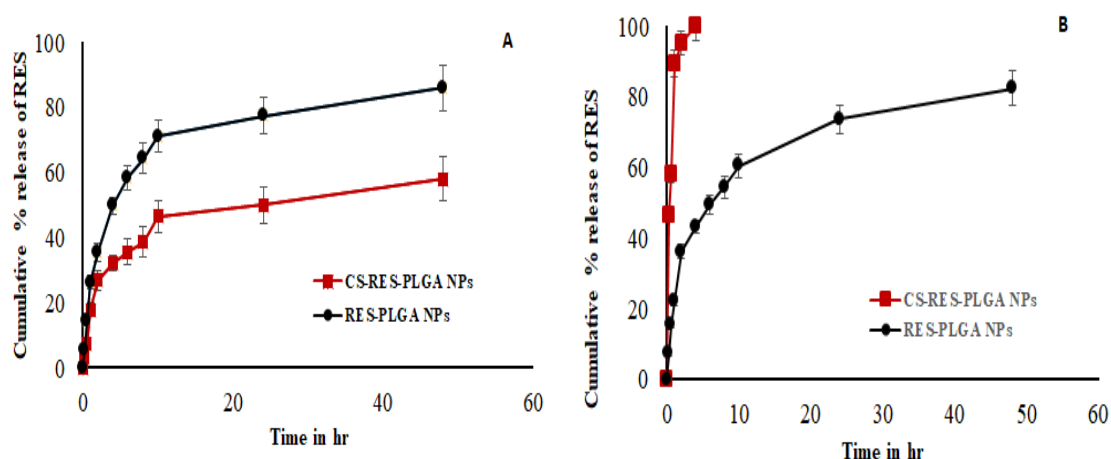


Figure 6. Photostability data obtained for RES and CS-RES-PLGA NPs.

The comparative photostability studies were done to evaluate the effectiveness of the encapsulation of RES in achieving chemical stability. The study was based on the fact that trans-RES gets converted to cis-RES on UV irradiation affecting its bioactivity [37]. The results were as expected from previous reports. It is known that even encapsulation of RES in PLGA alone imparts sufficient chemical stability compared to unencapsulated RES [20]. It is obvious that the PLGA polymer restricts the exposure of UV light to RES. It is noteworthy that this encapsulation enhanced water solubility and bioactivity of RES in addition to chemical stability. Such additional benefits are widely reported as the advantage of the encapsulation of RES [38]. Therefore, we could expect that an additional CS coating will further improve the chemical stability of RES. At all sampling points, the percent trans-RES remained was higher for the CS-RES-PLGA NPs than RES alone. Further, the difference between the percent trans-RES remained for the samples was found to increase with storage time. This was a clear indication of the protective effect of CS-coated PLGA NPs on the photodegradation of RES. Similar results were observed during the encapsulation of RES in other systems too such as lipid-based NPs and nanoemulsions [37].

### 3.6. In Vitro Release Characteristics from the NPs

The release of the entrapped therapeutic agent from the colloidal delivery system is essential to produce the intended response; this release can be effectively modulated through alteration of the physicochemical characteristics of the medium. As the formulated CS-coated RES-PLGA is intended to deliver the entrapped drug within the cancer microenvironment, the release study of the formulations was performed at pH 5.5 and 7.4, which approximately corresponds to the pH of the tumor microenvironment and different cellular compartments, respectively. Figure 7 clearly shows that the release of RES from the CS-coated PLGA NPs and PLGA NPs was 58.06% and  $85.97\% \pm 6.87\%$  respectively at pH 7.4. The PLGA NPs showed a burst release of 45.56% at 2 h, whereas CS-coated PLGA NPs showed only  $23.9\% \pm 3.1\%$  drug release. This demonstrates that the initial release of RES in CS-coated PLGA NPs was significantly ( $p < 0.05$ ) slower than that in PLGA NPs, with a more sustained release at pH 7.4. At pH 5.5 the release rate of RES in CS-coated PLGA NPs was very fast and 50% RES was released at 2 h, whereas PLGA NPs showed only  $22.3\% \pm 1.25\%$  drug release. This suggests that CS-coated PLGA NPs had pH-responsive properties. The pattern of RES release from our formulation is quite comparable from the findings in the literature, where the authors had demonstrated  $>60\%$  release of RES from the PLGA NPs within the time-frame of 24 h [13]. Furthermore, the slowing in release pattern of RES in the CS-coated PLGA NPs is in agreement with findings of Sanna and coworkers, where the authors demonstrated a controlled release pattern of RES following encapsulation of RES in CS-coated polymeric NPs [14]. The release of RES from the PLGA-NPs was found to be sustained over a period of 48 h, with a cumulative release of  $82.34\% \pm 6.73\%$  at pH 5.5.



**Figure 7.** In vitro release profiles of RES from RES-PLGA NPs and CS-coated RES-PLGA NPs at pH 7.4 (panel A) and at pH 5.5 (panel B) (The temperature was set at 37 °C, mean  $\pm$ SD,  $n = 3$ ).

Modulation of the release of the entrapped drug in any carrier is essential to avoid unfavorable side effects resulting from exposure of normal cells to the released drug. Therefore, the current formulation approach was planned to modulate the release of the entrapped drug (RES) within the cancer microenvironment. To accomplish this goal, we coated the RES-PLGA NPs with CS, which will primarily release the drug at the particular pH of the cancerous environment. It is relevant to mention that the pH of the cancer microenvironment is acidic and ranges from 5.5 to 7.0, due to hypoxic conditions during uncontrolled proliferation, deficient blood perfusion, and glycolytic cancer cell metabolism [39]. Therefore, to ensure the release of the entrapped drug within the acidic environment and decreased systemic exposure of the drug, we evaluated the release of the drug in two different pH values, 5.5 and 7.4, which roughly corresponds to the cancer environment and systemic circulation respectively. We showed that RES was rapidly released from the CS-coated RES-PLGA NPs in an acidic environment, whereas the release pattern at physiological pH was slow. Thus, we suggest that the

developed NP formulation would stay in the circulation without releasing the entrapped drug but would rapidly release RES at the site of action.

### 3.7. Antioxidant Activity of RES and CS-RES-PLGA NPs

The DPPH scavenging activity of the RES solution, CS-RES-PLGA NPs, and standard gallic acid was shown in Figure 8. The DPPH scavenging activity of gallic acid was increased linearly with increasing concentration from 5  $\mu\text{g/mL}$  ( $90.72\% \pm 2.14\%$ ) to 25  $\mu\text{g/mL}$  ( $97.71\% \pm 0.66\%$ ), and after increasing the concentration to 50  $\mu\text{g/mL}$  ( $97.94\% \pm 0.63\%$ ) there was no significant ( $p > 0.05$ ) increase in scavenging activity. The DPPH scavenging activity of RES and CS-RES-PLGA NPs was found to be increased with increasing RES concentration from 10 to 50  $\mu\text{g/mL}$ , but the RES NPs had a significantly ( $p < 0.05$ ) higher activity as compared to RES alone at all concentrations. These results indicating that the RES NPs more efficient at scavenging DPPH than the free RES. Application of PLGA has broadly been explored for controlled release properties of the entrapped drug. Limited information is available in the literature on the enhancement of the antioxidant activity of PLGA entrapped drugs, where few of the researchers reported that PLGA nanoformulations platform for enhanced functional properties [21]. Therefore, enhanced scavenging potential of DPPH free radicals by RES via CS-RES-PLGA NPs could be explained by the enhanced delivery system for phenolic compounds.

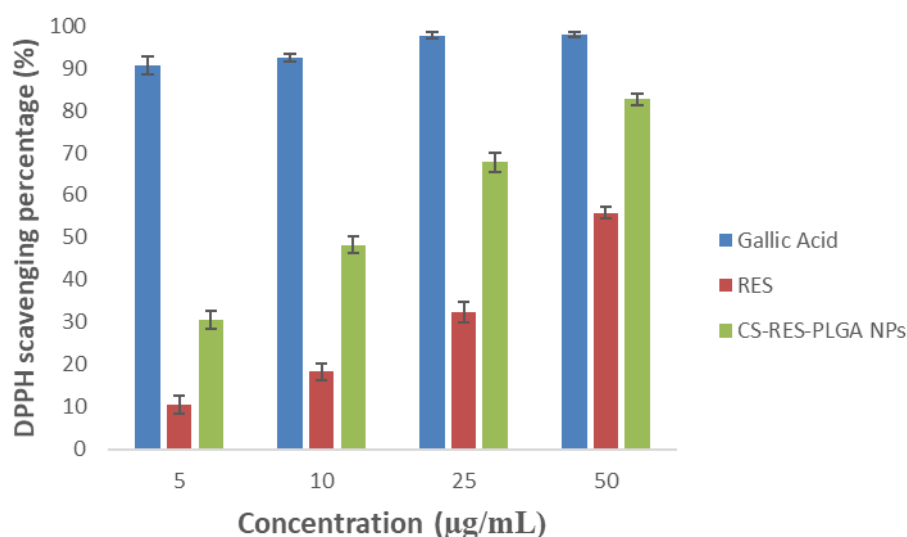


**Figure 8.** DPPH scavenging activity of free resveratrol, CS-RES-PLGA NPs and gallic acid at different concentrations. ( $p < 0.05$ ; RES vs. CS-RES-PLGA NPs).

### 3.8. Cytotoxicity of Prepared RES Nanoformulations

Keeping in view the importance of cytotoxic agents and corresponding cell death assays in cancer drug discovery [40] we evaluated the cytotoxic potential of RES, RES PLGA NPs, CS coated RES-PLGA NPs and blank CS coated PLGA NPs on the NSCLC cell line H1299. After 24 h, RES and its nano-formulation produced a concentration-dependent reduction in cell viability (Figure 9). Blank NPs did not show significant ( $p > 0.05$ ) cytotoxicity as compared to other nanoformulation. Further, overall cell death/cytotoxic effect/s (in terms of respective  $\text{IC}_{50}$  values) of RES ( $57.31 \pm 2.3 \mu\text{g/mL}$ ), RES-PLGA NPs ( $49.51 \pm 1.06$ ) and (CS coated RES-PLGA NPs ( $34.99 \pm 1.51 \mu\text{g/mL}$ ) were observed. CS coated RES-PLGA NPs showed a more pronounced and significant effect ( $p \leq 0.001$ ) compared to the drug RES and RES-PLGA NPs ( $p < 0.05$ ) (Figure 9), suggesting a better cytotoxic potential of RES when used as a nano-formulation. Taken together, these results suggest a better cytotoxic potential of CS coated PLGA NPs than RES and RES-PLGA NPs against the NSCLC cell line H1299.



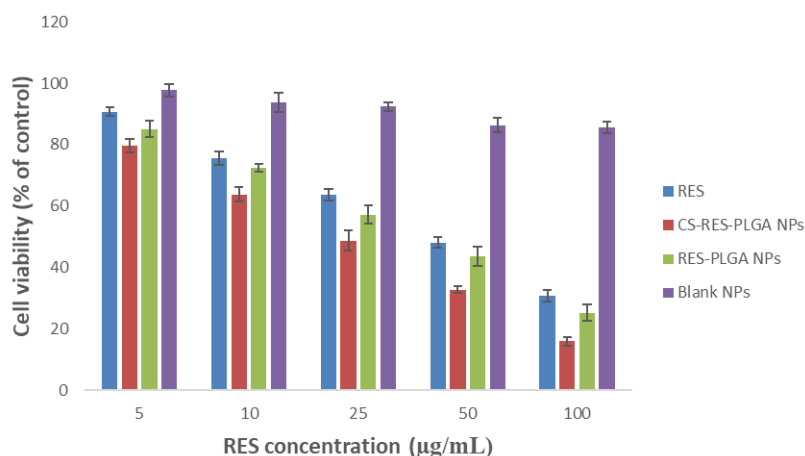


**Figure 9.** In vitro cytotoxicity of free RES, CS coated RES-PLGA NPs, RES-PLGA NPs and blank CS-coated PLGA NPs (blank NPs) in H1299 cells after 24 h incubation.

### 3.9. Induction of Apoptosis by Free RES and CS Coated RES-PLGA NPs (RES NPs)

To gain mechanistic insights on the cytotoxic effects of RES and its NP formulations, we evaluated their apoptotic potential on NSCLS cell line H1299 by flow cytometry, using Annexin V/FITC kit. It was found that RES (57.31 µg/mL/24 h) significantly ( $p < 0.05$ ) induced apoptotic cell death as compared to the untreated control group (Figure 10A,B). However, when H1299 cells were treated with RES-NP (34.99 µg/mL/24 h.), the extent of apoptosis was even more significantly ( $p < 0.05$ ) increased compared to both controls as well as RES treated groups (Figure 10 A–C). Both RES and RES-NPs also increased the necrotic cell number compared to the control group; however, the increase was not significant ( $p > 0.05$ ) (10D). Further, the percentage of early and late apoptotic cells (56.65%  $\pm$  2.2%) in the RES-treated group was significantly ( $p \leq 0.05$ ) lower than in the RES-NP-treated group (83.65%  $\pm$  20.5%), suggesting a strong apoptosis-inducing potential of the RES nano-formulation. The percentage of early apoptotic cells did not show much difference between RES (29.9%  $\pm$  0.56%) and RES-NPs (27.3%  $\pm$  8.76%) treated groups. However, there was a lower percentage of late apoptotic cells in the RES alone group (26.75%  $\pm$  9.26%) compared to RES-NPs (56.35%  $\pm$  9.68%), indicating that the RES-NPs has a strong apoptotic activity for cancerous cells compared to the free RES (Figure 10D).

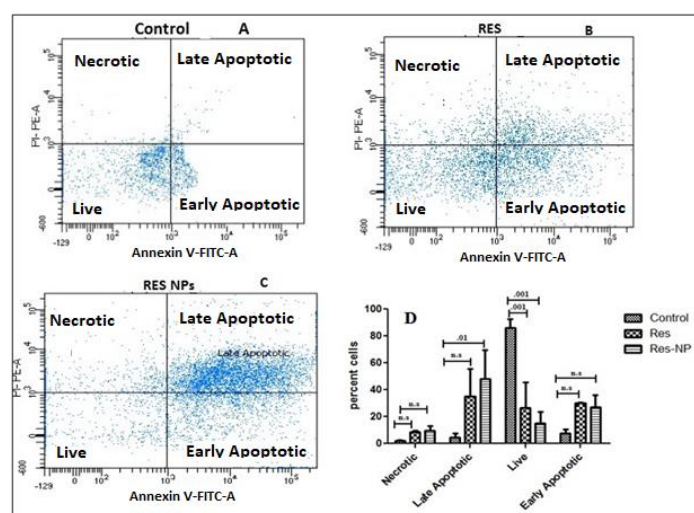


**Figure 10.** Flow cytometric dot plots of annexin V/PI staining are shown in (A) untreated H1299 cells (Control) (B) H1299 cells treated with RES (C) H1299 cells treated with RES NPs. (D): Flow cytometric analysis showed live cell, early apoptosis, late apoptosis and necrotic cells of free RES and RES NPs as compared to control.

### 3.10. Western Blotting

We next sought to evaluate the effect of RES and its NP formulations on apoptosis at the molecular level by studying the expression of pro- and anti-apoptotic proteins viz Bax and Bcl2, using Western blotting (Figure 11A,B). Both RES and the nanoformulations of RES significantly induced the expression of the pro-apoptotic protein Bax compared to the control group. However, the induction in Bax expression was greater in the RES-NPs group as compared RESs alone (Figure 11). Likewise, the anti-apoptotic Bcl2 protein was significantly reduced in both RES and RES-NPs treated groups compared to the control. However, the reduction did not show any significant difference between RES-NPs and RES alone (Figure 11A,B). Taken together, these results suggest a more potent apoptotic effect of RES-NPs than RES alone on NSCLS cell line H1299.

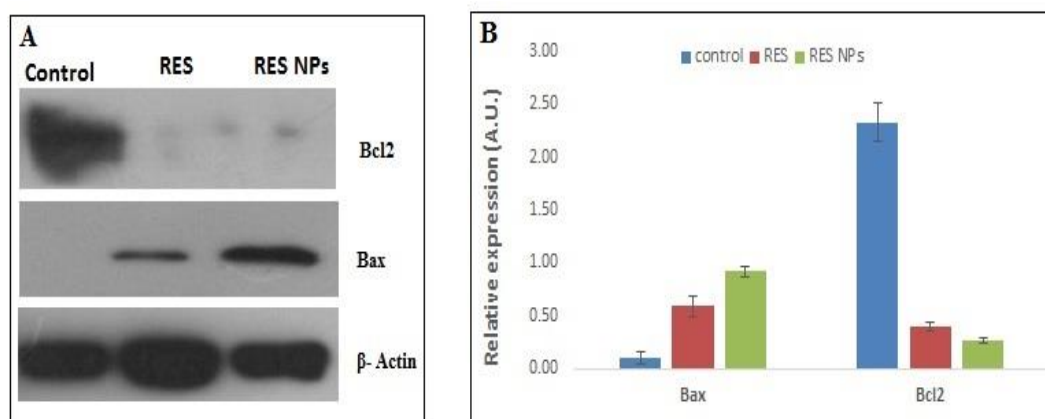


**Figure 11.** (A) Impact of control, free RES, and RES NPs formulations on protein expression of Bax and Bcl-2 levels in H1299 cells through western blotting. (B) Densitometric analysis of the bands representing the expression of Bax and Bcl2 was performed using image j software.

### 3.11. Effect of Free RES and RES-PLGA NPs on Cell Cycle Arrest

To determine whether apoptosis is related to cell cycle arrest, we subjected the free RES and RES NPs treated H1299 cells to propidium iodide (a DNA binding dye) staining and subsequent FACS analysis. In both free RES and RES NPs treated groups there was a significant ( $p \leq 0.05$ ) reduction in the proportion of cells in the G2/M phase, arresting the cell division, compared to the control group (Figure 12). Further, both RES ( $77.67\% \pm 13.04\%$ ) and its nano-formulation RES-NPs ( $84.64\% \pm 8.05\%$ ) showed a non-significant ( $p > 0.05$ ) arrest of cells in G0/G1 phase compared to the control group ( $74.9\% \pm 2.53\%$ ) (Figure 12). However, both RES ( $7.73\% \pm 4.33\%$ ) and RES-NPs ( $4.65 \pm 2.19$ ) treated cells showed a significant reduction ( $p \leq 0.05$ ) in the S phase compared to the control group ( $13.68\% \pm 2.8\%$ ). Such a reduction in the S phase automatically resulted in a reduction in the proportion of cells in the G2/M phase, as evident from the corresponding values for RES ( $2.56\% \pm 0.79\%$ ), RES-NPs ( $3.17\% \pm 0.38\%$ ) compared to control ( $14.5\% \pm 3.95\%$ ). Overall, the results suggest that both RES and RES NPs significantly ( $p \leq 0.05$ ) inhibited cell cycle progression; however, the overall effects are more pronounced in the RES NPs group than the free RES.

We evaluated the nano-formulation of RES to assess whether this nano-formulation enhances the anti-tumor effect of RES using the human NSCLC cell line H1299. We found that RES-NPs not only proved more cytotoxic than RES alone to the cancerous cells but also induced apoptosis in these cells, with an increased percentage of total apoptotic cells in RES-NPs group compared to both RES-only and control-treated cells. At the molecular level, RES-NPs were more effective in inducing pro-apoptotic Bax while reducing anti-apoptotic Bcl2 expression than RES alone or control NPs. In terms of cycle arrest, RES-NPs were more effective in inhibiting DNA synthesis as evidenced by the smaller percentage of cells in S phase compared to either Res or control groups. However, both RES-NPs as well as RES only groups arrested cells both at G1/S as well as G2/M phases compared to control-treated groups,

though there was no statistically significant ( $p > 0.05$ ) difference between the RES-NPs and RES only groups. Both RES, as well as its nano-formulation RES-NPs, showed concentration-dependent cell death in NSCLC cell line H1299. The smaller  $IC_{50}$  value of RES-NPs ( $34.99 \mu\text{g/mL}$ ) indicates its fairly greater potency compared to that of the RES-alone group ( $57.31 \mu\text{g/mL}$ ). The greater cytotoxic effect of RES-NPs may possibly be attributed to the small size and positive charge of the nano-formulation and its greater uptake by the H1299 cells [22] by facilitating its passive transport across the cell membrane compared to the RES only.

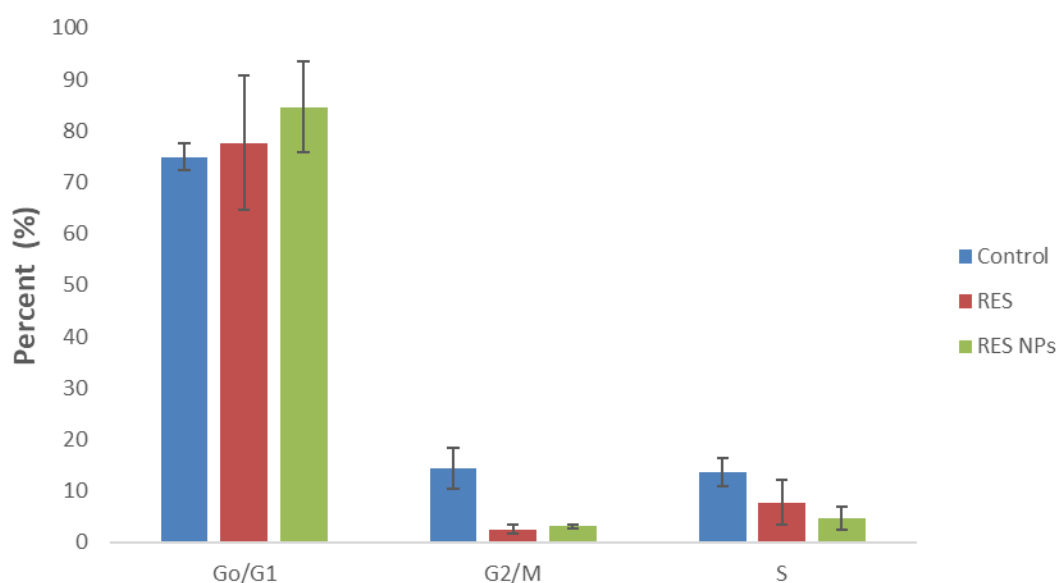


**Figure 12.** Flow cytometric analysis of the effect of RES and RES NPs in H1299 lung cancer cells at 24 h for cell cycle analysis. The data were analyzed using one-way ANOVA followed by Tukey's post hoc test. The percentage of cells in each group was compared with control,  $p < 0.05$  indicates a significant difference.

Apoptosis is a programmed cell death mechanism for removing cells with extensive DNA damage which otherwise may lead to various disease etiologies like cancer. Avoiding apoptosis is an established cancer hallmark; thus, sensitizing cancer cells towards apoptosis is an important aspect of cancer therapeutics [41]. We speculated that the increased cytotoxicity of the NPs formulation might be associated with the induction of apoptosis in H1299 cells. Previous studies have shown that RES induces cell death, possibly via apoptosis or autophagy [42]. We observed four types of cells after annexin V FITC/PI staining, these being live, necrotic, early and late apoptotic cells. Both RES and its nano-formulation RES-NPs activated the intrinsic apoptotic pathway, as evidenced by a well-marked induction of the pro-apoptotic protein Bax and a concomitant decrease in the anti-apoptotic protein Bcl2 [43] compared to the control. Such modulation of Bax/Bcl2 expression leads to cytochrome C release from mitochondria, in turn activating caspase-9 and hence caspase-3 to initiate apoptosis [44]. This could be one possible aspect of the mechanism/s responsible for increased cell death and apoptosis in response to RES or its nano-formulation RES-NPs; however, more studies are needed to establish this mechanism more comprehensively. Unrestrained proliferation, characteristic of a dysregulated cell cycle is one of the core hallmarks of cancer [45]; thus targeting this cell cycle progression has become a desirable trait for most anticancer therapies. When active, cancer cells tend to remain in a spontaneous division state characterized by an incessant transition between G1, S, G2 and M phases of the cell cycle. Contrary to this, in a non-transformed state, the cell cycle is regulated by specific checkpoints- G1/S (the state marks the entry to the synthesis phase) and G2/M (the state which marks the entry into the active mitotic phase). We found that both RES as well its nano-formulation RES-NPs significantly ( $p < 0.05$ ) arrested the cells at G1/S and G2/M transitions, indicating a strong

DNA damaging mechanism of inducing cell death [46]. Further, the smaller proportion of cells in the S-phase in response to treatment with RES-NPs ( $4.65\% \pm 2.19\%$ ) compared to either RES alone ( $7.73\% \pm 4.33\%$ ) or control ( $13.68\% \pm 2.80\%$ ) indicates a more promising DNA damage induced by the nano-formulation during G1 than that induced by RES alone [46]. Previous reports also suggest that RES induces cell cycle arrest either at G1 [47] or by blocking G1/S transition and inhibiting G2/M progression [48], thus further supporting our results.

#### 4. Conclusions

CS coated PLGA NPs of RES was successfully developed and characterized. The effect of CS and cryoprotectant concentration on PS, PDI, and ZP were studied. The prepared NPs size and PDI were satisfactory and RES entrapment efficiency was found 75%. The stability of RES loaded PLGA NPs was improved by CS coating. TEM and SEM showed uniform particle distribution with a smooth surface and spherical shape. The CS coating provides modulation of in vitro drug release and showed a sustained release pattern. The positive zeta potential of the CS-coated NPs supports the binding of the nanocarrier to the negative surface of cancer cells to increase the cytotoxicity and enhance the apoptotic activity of formulation when compared with free RES. The chitosan-coated RES-PLGA NPs had a higher antioxidant effect than the free RES. Therefore, CS coated PLGA NPs of RES could be a potential nanocarrier to overcome the limitations of RES and improved therapeutic application.

**Author Contributions:** Conceptualization, supervision, funding acquisition: H.M.A., S.M. and N.A.A.; methodology, resources and data curation: M.H., S.M., R.P.; writing—original draft preparation and editing: H.M.A., S.M. and M.H. All authors have read and agreed to the published version of the manuscript.

**Funding:** This project was funded by the Deanship of Scientific Research (DSR) at King Abdulaziz University, Jeddah, under grant No. 1-166-36-HiCi.

**Acknowledgments:** The authors, therefore, acknowledge with thanks DSR for technical and financial support. The authors are thankful to Brian L. Furman (University of Strathclyde, Glasgow, UK) for critical reading of the manuscript and language editing.

**Conflicts of Interest:** The authors declare no conflict of interest.

#### References

1. Amri, A.; Chaumeil, J.C.; Sfar, S.; Charrueau, C. Administration of resveratrol: What formulation solutions to bioavailability limitations? *J. Control. Release* **2012**, *158*, 182–193. [\[CrossRef\]](#) [\[PubMed\]](#)
2. Sessa, M.; Balestrieri, M.L.; Ferrari, G.; Servillo, L.; Castaldo, D.; D’Onofrio, N.; Donsì, F.; Tsao, R. Bioavailability of encapsulated resveratrol into nanoemulsion-based delivery systems. *Food Chem.* **2014**, *147*, 42–50. [\[CrossRef\]](#) [\[PubMed\]](#)
3. Richard, T.; Pawlus, A.D.; Iglésias, M.-L.; Pedrot, E.; Waffo-Teguo, P.; Mérillon, J.-M.; Monti, J.-P. Neuroprotective properties of resveratrol and derivatives. *Ann. N. Y. Acad. Sci.* **2011**, *1215*, 103–108. [\[CrossRef\]](#) [\[PubMed\]](#)
4. Ha, E.S.; Sim, W.Y.; Lee, S.K.; Jeong, J.S.; Kim, J.S.; Baek, I.H.; Choi, D.H.; Park, H.; Hwang, S.J.; Kim, M.S. Preparation and evaluation of resveratrol-loaded composite nanoparticles using a supercritical fluid technology for enhanced oral and skin delivery. *Antioxidants* **2019**, *8*, 554. [\[CrossRef\]](#)
5. She, Q.B.; Bode, A.M.; Ma, W.Y.; Chen, N.Y.; Dong, Z. Resveratrol-induced activation of p53 and apoptosis is mediated by extracellular-signal-regulated protein kinases and p38 kinase. *Cancer Res.* **2001**, *61*, 1604–1610.
6. Walle, T.; Hsieh, F.; DeLegge, M.H.; Oatis, J.E.; Walle, U.K. High absorption but very low bioavailability of oral resveratrol in humans. *Drug Metab. Dispos.* **2004**, *32*, 1377–1382. [\[CrossRef\]](#)
7. Choudhury, H.; Pandey, M.; Yin, T.H.; Kaur, T.; Jia, G.W.; Tan, S.Q.L.; Weijie, H.; Yang, E.K.S.; Keat, C.G.; Bhattamishra, S.K.; et al. Rising horizon in circumventing multidrug resistance in chemotherapy with nanotechnology. *Mater. Sci. Eng. C* **2019**, *101*, 596–613. [\[CrossRef\]](#)
8. Guo, L.; Peng, Y.; Li, Y.; Yao, J.; Zhang, G.; Chen, J.; Wang, J.; Sui, L. Cell death pathway induced by resveratrol-bovine serum albumin nanoparticles in a human ovarian cell line. *Oncol. Lett.* **2015**, *9*, 1359–1363. [\[CrossRef\]](#)

9. Karthikeyan, S.; Prasad, R.R.; Ganamani, A.; Balamurugan, E. Anticancer activity of resveratrol-loaded gelatin nanoparticles on NCI-H460 non-small cell lung cancer cells. *Biomed. Prev. Nutr.* **2013**, *3*, 64–73. [[CrossRef](#)]
10. Wang, W.; Zhang, L.; Chen, T.; Guo, W.; Bao, X.; Wang, D.; Ren, B.; Wang, H.; Li, Y.; Wang, Y.; et al. Anticancer Effects of Resveratrol-Loaded Solid Lipid Nanoparticles on Human Breast Cancer Cells. *Molecules* **2017**, *22*, 1814. [[CrossRef](#)]
11. Nassir, A.M.; Shahzad, N.; Ibrahim, I.A.A.; Ahmad, I.; Md, S.; Ain, M.R. Resveratrol-loaded PLGA nanoparticles mediated programmed cell death in prostate cancer cells. *Saudi Pharm. J.* **2018**, *26*, 876–885. [[CrossRef](#)] [[PubMed](#)]
12. Fathi, M.; Zangabad, P.S.; Majidi, S.; Barar, J.; Erfan-Niya, H.; Omid, Y. Stimuli-responsive chitosan-based nanocarriers for cancer therapy. *BioImpacts* **2017**, *7*, 269–277. [[CrossRef](#)] [[PubMed](#)]
13. Miele, D.; Catenacci, L.; Sorrenti, M.; Rossi, S.; Sandri, G.; Malavasi, L.; Dacarro, G.; Ferrari, F.; Bonferoni, M.C. Chitosan oleate coated poly lactic-glycolic acid (PLGA) nanoparticles versus chitosan oleate self-assembled polymeric micelles, loaded with resveratrol. *Mar. Drugs* **2019**, *17*, 515. [[CrossRef](#)] [[PubMed](#)]
14. Sanna, V.; Roggio, A.M.; Siliani, S.; Piccinini, M.; Marceddu, S.; Mariani, A.; Sechi, M. Development of novel cationic chitosan- and anionic alginate-coated poly(D,L-lactide-co-glycolide) nanoparticles for controlled release and light protection of resveratrol. *Int. J. Nanomed.* **2012**, *7*, 5516.
15. Wang, X.; Li, G.; Zhang, P.; Li, W.; He, X. Surface engineering of resveratrol to improve neuro-protection and functional recovery after spinal cord injury in rat. *J. Drug Deliv. Sci. Technol.* **2019**, *49*, 89–96. [[CrossRef](#)]
16. Budhian, A.; Siegel, S.J.; Winey, K.I. Controlling the in vitro release profiles for a system of haloperidol-loaded PLGA nanoparticles. *Int. J. Pharm.* **2008**, *346*, 151–159. [[CrossRef](#)]
17. Md, S.; Alhakamy, N.A.; Aldawsari, H.M.; Asfour, H.Z. Neuroprotective and antioxidant effect of naringenin-loaded nanoparticles for nose-to-brain delivery. *Brain Sci.* **2019**, *9*, 275. [[CrossRef](#)]
18. Pandey, M.; Choudhury, H.; Gunasegaran, T.A.P.; Nathan, S.S.; Md, S.; Gorain, B.; Tripathy, M.; Hussain, Z. Hyaluronic acid-modified betamethasone encapsulated polymeric nanoparticles: Fabrication, characterisation, in vitro release kinetics, and dermal targeting. *Drug Deliv. Transl. Res.* **2019**, *9*, 520–533. [[CrossRef](#)]
19. Ahmadi Nasab, N.; Hassani Kumleh, H.; Beygzadeh, M.; Teimourian, S.; Kazemzad, M. Delivery of curcumin by a pH-responsive chitosan mesoporous silica nanoparticles for cancer treatment. *Artif. Cells Nanomed. Biotechnol.* **2018**, *46*, 75–81. [[CrossRef](#)]
20. Wan, S.; Zhang, L.; Quan, Y.; Wei, K. Resveratrol-loaded PLGA nanoparticles: Enhanced stability, solubility and bioactivity of resveratrol for non-alcoholic fatty liver disease therapy. *R. Soc. Open Sci.* **2018**, *5*, 181457. [[CrossRef](#)]
21. Pereira, M.C.; Oliveira, D.A.; Hill, L.E.; Zambiasi, R.C.; Borges, C.D.; Vizzotto, M.; Mertens-Talcott, S.; Talcott, S.; Gomes, C.L. Effect of nanoencapsulation using PLGA on antioxidant and antimicrobial activities of guabiroba fruit phenolic extract. *Food Chem.* **2018**, *240*, 396–404. [[CrossRef](#)] [[PubMed](#)]
22. Alhakamy, N.A.; Shadab, M. Repurposing itraconazole loaded PLGA nanoparticles for improved antitumor efficacy in non-small cell lung cancers. *Pharmaceutics* **2019**, *11*, 685. [[CrossRef](#)]
23. Min, J.; Shen, H.; Xi, W.; Wang, Q.; Yin, L.; Zhang, Y.; Yu, Y.; Yang, Q.; Wang, Z.-N. Synergistic anticancer activity of combined use of caffeic acid with paclitaxel enhances apoptosis of non-small-cell lung cancer H1299 cells in vivo and in vitro. *Cell. Physiol. Biochem.* **2018**, *48*, 1433–1442. [[CrossRef](#)] [[PubMed](#)]
24. Lu, B.; Lv, X.; Le, Y. Chitosan-modified PLGA nanoparticles for control-released drug delivery. *Polymers* **2019**, *11*, 304. [[CrossRef](#)] [[PubMed](#)]
25. Ho, H.N.; Tran, T.H.; Tran, T.B.; Yong, C.S.; Nguyen, C.N. Optimization and characterization of artesunate-loaded chitosan-decorated poly(D,L-lactide-co-glycolide) acid nanoparticles. *J. Nanomater.* **2015**, *2015*, 674175. [[CrossRef](#)]
26. Al-Nemrawi, N.K.; Okour, A.R.; Dave, R.H. Surface modification of PLGA nanoparticles using chitosan: Effect of molecular weight, concentration, and degree of deacetylation. *Adv. Polym. Technol.* **2018**, *37*, 3066–3075. [[CrossRef](#)]
27. Almalik, A.; Alradwan, I.; Kalam, M.A.; Alshamsan, A. Effect of cryoprotection on particle size stability and preservation of chitosan nanoparticles with and without hyaluronate or alginate coating. *Saudi Pharm. J.* **2017**, *25*, 861–867. [[CrossRef](#)]
28. Abdelwahed, W.; Degobert, G.; Stainmesse, S.; Fessi, H. Freeze-drying of nanoparticles: Formulation, process and storage considerations. *Adv. Drug Deliv. Rev.* **2006**, *58*, 1688–1713. [[CrossRef](#)]



29. Abdelwahed, W.; Degobert, G.; Fessi, H. A pilot study of freeze drying of poly(epsilon-caprolactone) nanocapsules stabilized by poly(vinyl alcohol): Formulation and process optimization. *Int. J. Pharm.* **2006**, *309*, 178–188. [[CrossRef](#)]
30. Konan, Y.N.; Gurny, R.; Allémann, E. Preparation and characterization of sterile and freeze-dried sub-200 nm nanoparticles. *Int. J. Pharm.* **2002**, *233*, 239–252. [[CrossRef](#)]
31. Date, P.V.; Samad, A.; Devarajan, P.V. Freeze thaw: A simple approach for prediction of optimal cryoprotectant for freeze drying. *AAPS PharmSciTech* **2010**, *11*, 304–313. [[CrossRef](#)] [[PubMed](#)]
32. Katas, H.; Hussain, Z.; Rahman, S.A. Storage stabilisation of albumin-loaded chitosan nanoparticles by lyoprotectants. *Trop. J. Pharm. Res.* **2013**, *12*, 135–142. [[CrossRef](#)]
33. Rampino, A.; Borgogna, M.; Blasi, P.; Bellich, B.; Cesàro, A. Chitosan nanoparticles: Preparation, size evolution and stability. *Int. J. Pharm.* **2013**, *455*, 219–228. [[CrossRef](#)] [[PubMed](#)]
34. Abd El Hady, W.E.; Mohamed, E.A.; Soliman, O.A.E.-A.; El-Sabbagh, H.M. In vitro-in vivo evaluation of chitosan-PLGA nanoparticles for potentiated gastric retention and anti-ulcer activity of diosmin. *Int. J. Nanomed.* **2019**, *14*, 7191–7213. [[CrossRef](#)] [[PubMed](#)]
35. Al-Nemrawi, N.; Alshraideh, N.; Zayed, A.; Altaani, B. Low molecular weight chitosan-coated PLGA nanoparticles for pulmonary delivery of tobramycin for cystic fibrosis. *Pharmaceuticals* **2018**, *11*, 28. [[CrossRef](#)] [[PubMed](#)]
36. Luangtana-Anan, M.; Limmatvapirat, S.; Nunthanid, J.; Chalongsuk, R.; Yamamoto, K. Polyethylene glycol on stability of chitosan microparticulate carrier for protein. *AAPS PharmSciTech* **2010**, *11*, 1376–1382. [[CrossRef](#)]
37. Neves, A.R.; Martins, S.; Segundo, M.A.; Reis, S. Nanoscale delivery of resveratrol towards enhancement of supplements and nutraceuticals. *Nutrients* **2016**, *8*, 131. [[CrossRef](#)]
38. Koga, C.C.; Andrade, J.E.; Ferruzzi, M.G.; Lee, Y. Stability of trans-resveratrol encapsulated in a protein matrix produced using spray drying to UV light stress and simulated gastro-intestinal digestion. *J. Food Sci.* **2016**, *81*, C292–C300. [[CrossRef](#)]
39. Justus, C.R.; Dong, L.; Yang, L.V. Acidic tumor microenvironment and pH-sensing G protein-coupled receptors. *Front. Physiol.* **2013**, *4*, 354. [[CrossRef](#)]
40. Bahuguna, A.; Khan, I.; Bajpai, V.K.; Kang, S.C. MTT assay to evaluate the cytotoxic potential of a drug. *Bangladesh J. Pharmacol.* **2017**, *12*, 115–118. [[CrossRef](#)]
41. Kerr, J.F.R.; Wyllie, A.H.; Currie, A.R. Apoptosis: A basic biological phenomenon with wide-ranging implications in tissue kinetics. *Br. J. Cancer* **1972**, *26*, 239–257. [[CrossRef](#)]
42. Fan, Y.; Chiu, J.-F.; Liu, J.; Deng, Y.; Xu, C.; Zhang, J.; Li, G. Resveratrol induces autophagy-dependent apoptosis in HL-60 cells. *BMC Cancer* **2018**, *18*, 581. [[CrossRef](#)]
43. Zaman, S.; Wang, R.; Gandhi, V. Targeting the apoptosis pathway in hematologic malignancies. *Leuk. Lymphoma* **2014**, *55*, 1980–1992. [[CrossRef](#)] [[PubMed](#)]
44. Lin, W.; Xie, J.; Xu, N.; Huang, L.; Xu, A.; Li, H.; Li, C.; Gao, Y.; Watanabe, M.; Liu, C.; et al. Glucocalyxin A induces G2/M cell cycle arrest and apoptosis through the PI3K/Akt pathway in human bladder cancer cells. *Int. J. Biol. Sci.* **2018**, *14*, 418–426. [[CrossRef](#)] [[PubMed](#)]
45. Hanahan, D.; Weinberg, R.A. Hallmarks of cancer: The next generation. *Cell* **2011**, *144*, 646–674. [[CrossRef](#)] [[PubMed](#)]
46. Tyagi, A.K.; Singh, R.P.; Agarwal, C.; Chan, D.C.; Agarwal, R. Silibinin strongly synergizes human prostate carcinoma DU145 cells to doxorubicin-induced growth inhibition, G(2)-M arrest, and apoptosis. *Clin. Cancer Res.* **2002**, *8*, 3512–3519.
47. Ahmad, N.; Adhami, V.M.; Afaq, F.; Feyes, D.K.; Mukhtar, H. Resveratrol causes WAF-1/p21-mediated G1-phase arrest of cell cycle and induction of apoptosis in human epidermoid carcinoma A431 cells. *Clin. Cancer Res.* **2001**, *7*, 1466–1473.
48. Singh, S.K.; Banerjee, S.; Acosta, E.P.; Lillard, J.W.; Singh, R. Resveratrol induces cell cycle arrest and apoptosis with docetaxel in prostate cancer cells via a p53/p21 WAF1/CIP1 and p27 KIP1 pathway. *Oncotarget* **2017**, *8*, 17216–17228. [[CrossRef](#)]

